

# A hierarchical distributed control architecture for CHB converter with Integrated Battery Energy Storage

Jothi M Lexmi Devi <sup>1,\*</sup>, Sharly R A <sup>2</sup>

<sup>1</sup> ME Student, Department of PSE, Maria College of Engineering and Technology, Attoor

<sup>2</sup> Assistant professor, Department of PSE, Maria College of Engineering and Technology, Attoor

**Abstract**— Cascaded H-bridge topology has been used in grid tied converters for battery energy storage system due to its modular structure. To fully utilize the converter's modularity, this paper proposes a hierarchical distributed control architecture that consists of primary control, secondary control and battery state of charge (SOC) balancing control. Primary control ensures accurate current tracking while a distributed secondary control based on consensus algorithm is presented to regulate power sharing among modules and is proved to be stable theoretically. A distributed SOC balancing control is further introduced to improve energy efficiency of battery energy storage system. Finally, the hierarchical distributed control strategy is implemented using hardware controllers and a software platform. Besides, a carrier phase shift control is also implemented to achieve multilevel output voltage and harmonic reduction. The experimental results demonstrate the performance of the proposed control scheme effectively.

**Keywords**—: *Battery SOC balancing, cascaded H-bridge, consensus algorithm, distributed control.*

## I. INTRODUCTION

The increasing penetration of intermittent renewable energy sources, such as wind and solar, leads to numerous challenges for power grid operation. Dispatchable battery energy storage system (BESS) can address many of these issues by balancing out power fluctuation, shaving peak and filling valley in power requirement, increasing the reserve capacity of power grid, etc. As one of the most popular multilevel topologies, cascaded H-bridge (CHB) topology can effectively integrate BESS into the grid in medium voltage and high power applications, since it can use switching devices with lower voltage ratings and achieve low electromagnetic interference, low total harmonic distortion and fault-tolerance capability [1], [2]. Moreover, the modular structure of CHB topology makes it possible to achieve high conversion efficiency. CHB converter usually utilizes a central controller since it is easy to realize system control and synchronized modulation [3], [4]. The central controller

communicates with every Hbridge module via high-speed communication links. It executes all the calculations and sends switching commands to each module at every switching cycle, which increases the computational burden of the central controller and makes modularization difficult. Besides, the switching noise of high power converters can degrade the quality of communication, which could potentially degrade the converter's performance.

To circumvent the need for a central controller and high bandwidth communication, distributed control approaches are preferred. In distributed control strategies, the control and modulation are implemented in the local controllers of each module. Information is collected locally and exchanged through a sparse communication network. However, for CHB converter, it is challenging to achieve accurate output current regulation and power sharing control among modules without globally coordinating the switching actions of all the semiconductor devices. Existing distributed control strategies for the CHB converter is summarized in Table I. One approach is to directly regulate the current through one (or multiple) modules, while the remaining modules only operating in the open-loop and provide grid voltage support; such a method leads to a control architecture without communication [5]– [8]. In [9], a current controller hybrid automata is proposed to choose one module to regulate current at a time. However, the power output in each module cannot be regulated with the above methods and only a single module (or part of the modules) is used to compensate for all the transients or power variations, which may limit the converter operating range. To achieve both simultaneous regulations of both output current and power sharing through all the modules together, a method proposed in [10] is to optimize current regulation in module controllers by mitigating current measurement errors and DC voltage mismatches. But module controllers with the same control objective could be conflicting, as errors and mismatches could not be eliminated completely. Another commonly used control strategy is to add an output LC filter to each module so that each module can control its output voltage independently as an

AC signal instead of a pulse signal [11]– [14]. Extra LC filters eliminate the need of coordinating all the modules at the switching level, which in turn eliminates the need for high speed communication link. The control strategy in [11] utilizes the local voltage controller along with a virtual droop resistance in each module, but it requires a resistive impedance to connect to the grid.

In this paper, we extend the work in [12] and present an improved distributed architecture consists of three levels, namely primary control, secondary control, and battery SOC balancing control, respectively. The hierarchical distributed control architecture realizes all desirable features for the grid-tied CHB converter mentioned in the literature review. We use decentralized primary control to guarantee good current tracking performance. The secondary control based on consensus algorithm is improved to achieve the desired output voltage and power sharing regulation among modules. Our control algorithm has no need for an output LC filter and reduces the requirement on the communication network among modules compared with centralized control strategies. A sparse communication network with low bandwidth communication frequency is sufficient. Moreover, system stability analysis for power control level is performed to ensure the stability of the proposed distributed control. Considering the application of BESS, the secondary power control is further utilized to balance battery SOC. Additionally, a novel software platform, Resilient Information Architecture Platform for Smart Systems (RIAPS), is used to implement the proposed distributed control scheme and achieve the carrier phase shift (CPS) control between modules.

Three main technical contributions are presented in this paper. First, we apply the consensus algorithm for CHB converter to realize proportional power sharing regulation of each module. The proposed algorithm only needs sparse communication among neighboring modules. Although consensus algorithm has been widely used in microgrid control, to our best knowledge, it has not been applied for CHB converter control. Second, we provide the stability proof of the proposed control scheme. Third, we extend the secondary power control to realize the battery SOC balancing. Experiment results are provided to validate the proposed control scheme.

## II. LITERATURE SURVEY

Authors in [13] proposed a decentralized control strategy, where by emulating a virtual resistive output impedance in each module, the active and reactive power output of each module is regulated by dynamically updating the amplitude and phase of its output voltage, respectively. However, the controller coefficient needs to be properly designed to ensure sufficient damping for the overall stability of the entire system. In [14], a power factor-frequency inverse droop control strategy is proposed to generate the desired voltage reference, which does not need any communication. Power sharing among modules is realized when all the modules have the same phase angle. However, This method only works for standalone inverter and cannot be applied to grid-tied applications.

For the CHB converter with integrated BESS, it is necessary to inject a current with good quality into the grid while maintaining a desired output power ratio among modules. As the battery state of charge (SOC) of different modules may diverge from each other due to different operation demands, self-discharging rates, operating temperatures, etc, the ability of distributing different output power ratios among modules is important to balancing the SOC of modules. This can improve the energy utilization and extend the operating life of the BESS. Existing strategies of power and battery SOC control for CHB-BESS generally require that each module communicates with all the other modules to exchange information [15]–[17].

He et al. [18] proposed the inverse power factor control, which enables synchronization and power-sharing. Sun et al. [19] analyzed the power transmission characteristics and proposed an f-P/Q control with wider application to resistor-capacitor (RC) loads. A fully decentralized control method has been proposed for grid-connected modes [20], which uses droop scheme control to realize the synchronization between modules. However, these decentralized methods have not taken the characteristics and function into account, such as offering inertia control for friendly grid connections and achieving SOC balance in each battery module. To achieve these, many researchers have been focusing on battery characteristics and their functions in grid or renewable systems.

Different initial SOC values and operation states lead to SOC unbalancing, which has adverse effects on battery life and operational safety. To address this issue, Maharjan et al. proposed an SOC balancing method with zero-sequence

voltage injection for a three-phase cascaded H-bridge BESS. However, it relies on the central controller and cannot be applied to a singlephase cascaded H-bridge BESS. A hierarchical control [21], based on a central controller, has been proposed for frequency/voltage regulation and SOC balancing. To reduce computation load and communication burden, Shi et al. [22] proposed a decentralized method for SOC balance without communication in an islanded mode. However, with only local information, SOC balancing can be achieved with a low transient response, and the additional modification for SOC balancing can induce additional frequency deviation. In a grid-connected mode, this method is invalid for the fixed frequency limited by the grid. Xu et al. proposed a distributed control for a cascaded H-bridge BESS in a grid-connected mode. This method can achieve accuracy in active and reactive power distribution and SOC balancing. However, frequency synchronization still relies on synchronized modulation and does not consider frequency inertial support capability.

### III SYSTEM OVERVIEW

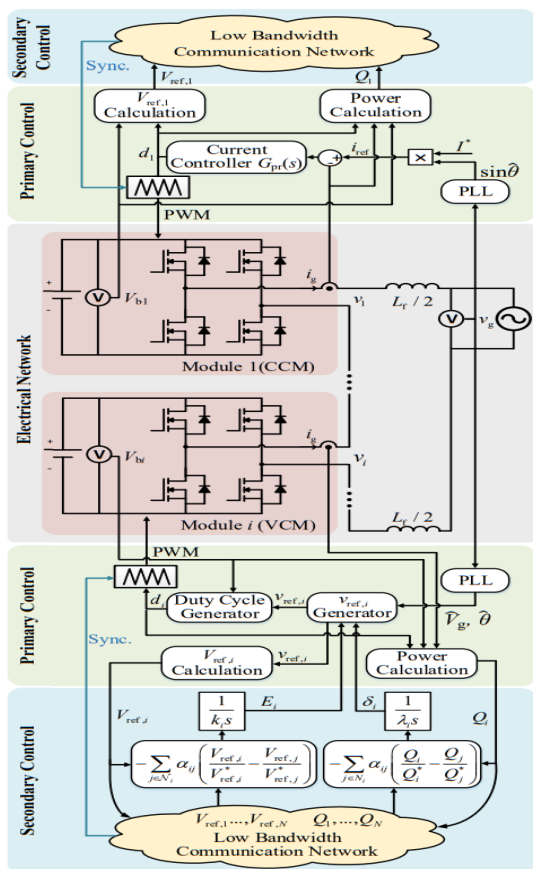


Fig 1 Circuit Diagram

A single-phase CHB converter with integrated batteries and its control block diagram are shown in Fig.1. It has N Hbridge modules connected in series with a filter inductor  $L_f$ . As the fundamental level of the proposed distributed control architecture, primary control maintains a stable and accurate current tracking. The corresponding control scheme is depicted in the primary control part of Fig.1

### IV PROPOSED SCHEMES

#### Primary Control Scheme

In primary control, one single module, i.e. module 1 in Fig. 1, is named as current control module (CCM) and controls the converter output current  $i_g$ . A digital phase lock loop (PLL) produces a grid synchronized reference sine signal  $\sin \hat{\theta}$ . The output current reference  $i_{ref}$  is generated by multiplying the current amplitude reference,  $I^*$  with the sine signal  $\sin \hat{\theta}$ . The output current  $i_g$  is then regulated by a PR controller. The current control block diagram is shown in Fig. 2. In s domain, the duty cycle of CCM can be written as:

$$d_1(s) = \left( k_p + \frac{2k_r\omega_c s}{s^2 + 2\omega_c s + \omega^2} \right) (i_{ref}(s) - i_g(s))$$

where  $k_p, k_r, \omega_c$ , are parameters of the PR controller. Due to the series connection, all modules share the same current, and simultaneous regulation of the current by two or more modules could destabilize the system. Therefore, only one CCM is allowed, while the other modules, i.e. module  $i$  ( $i = 2, 3, \dots, N$ ) in Fig. 1, are controlled in an open-loop manner. These modules are called voltage control module (VCM).

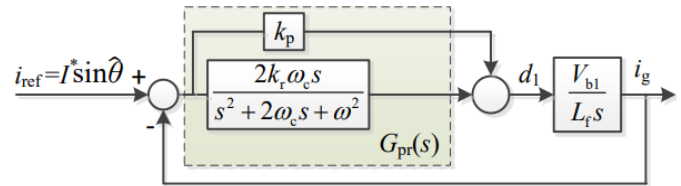


Fig. 2: The current control block diagram in the primary control

The reference output voltage for each VCM is designed as,

$$v_{ref,i} = \frac{1}{N} v_g = \frac{\hat{V}_g}{N} \sin \hat{\theta}$$

where  $\hat{V}_g$  and  $\hat{\theta}$  are grid voltage amplitude and phase tracked by PLL, respectively. In steady state, all the VCMs' output voltage build up a total fundamental AC voltage  $v_g(N-1)/N$ . The remained voltage mismatch  $v_g/N$  and the voltage drop across filter inductance  $v_{L_f}$  are compensated by the CCM.

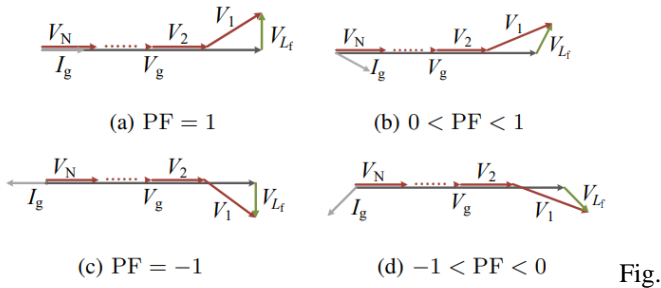


Fig.

3: The voltage vector diagram of different modules with only primary control under different conditions

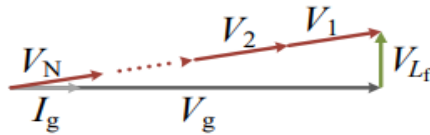


Fig.4: The voltage vector diagram under balanced condition

The desired fundamental component of CCM output voltage in steady state is,

$$v_1 = \frac{1}{N}v_g + v_{L_f} = \frac{1}{N}v_g + j\omega L_f i_g$$

Fig. 3.3 shows the voltage vector diagram of different modules with only primary control under different conditions. Fig. 3a shows the nominal operation condition at unity power factor (PF). VCMs have the same output voltage in the same phase of grid voltage, and the output voltage of CCM differs due to the filter inductor. If PF changes, the amplitude and phase of the output voltage for CCM change accordingly while the VCMs' output voltage remains unchanged, as shown in Fig. 3b-d. The output voltages of VCMs are aligned with grid voltage while the CCM compensates for voltage transients and voltage drop on the filter inductor. Therefore, CCM injects/absorbs different active and reactive power to/from the grid compared with VCMs.

Graph Theory and Consensus Algorithm Preliminaries

A communication network can be modeled by an undirected graph  $G = (V, \mathcal{E})$ , with  $V = \{n_1, n_2, \dots, n_N\}$  being the set of nodes,  $\mathcal{E} \subseteq \{(n_i, n_j) \in V \times V\}$  being the set of edges. Define  $\mathcal{A}$  as a corresponding  $N \times N$  adjacency matrix with  $\alpha_{ij} = \alpha_{ji} > 0$  if and only if the  $i$ th and  $j$ th node can communicate directly with each other, i.e.,  $(n_i, n_j) \in \mathcal{E}$ , otherwise  $\alpha_{ij} = \alpha_{ji} = 0$ . The indices of the nodes that are interconnected to node  $n_i$  directly form its neighboring set, denoted by  $N_i = \{j \mid (n_i, n_j) \in \mathcal{E}\}$ . If a path exists between any two nodes, it is called a connected graph.

Each node  $n_i$  ( $i = 1, 2, \dots, N$ ) of the graph represents an agent that holds a state  $x_i$ . To achieve consensus of a multiagent system (MAS), consensus algorithms can be used,

$$\dot{x}_i = - \sum_{j \in N_i} \alpha_{ij} (x_i - x_j)$$

For a connected graph  $G = (V, \mathcal{E})$ , when consensus is achieved, all state variables  $x_i$  converge to a common value, i.e.,  $x_i = x_j$  for any  $i$  and  $j$

If one leading agent is controlled by an external controller without obeying (4), while other agents still obey (4), it sets up a "leader-follower" relationship in consensus algorithm. In this case, the states of the agents can be controlled by regulating the motion of the leader agent

A. Secondary Control and Proportional Power Sharing

We use an undirected and connected graph  $G = (V, \mathcal{E})$  to model the communication network of the CHB converter. Every agent represents a module, and the edge depicts the communication channel among modules.

The proposed secondary control scheme is depicted in the secondary control part of Fig.1 and it exploits the "leader-follower" relationship in the consensus algorithm. The CCM acts as the leader and controls the converter output current, whereas VCMs act as followers and regulate the output voltage by:

$$\begin{aligned}
 v_{ref,i} &= \left( \frac{\hat{V}_g}{N} + E_i \right) \sin(\hat{\theta} + \delta_i) \\
 k_i \frac{dE_i}{dt} &= - \sum_{j \in \mathcal{N}_i} \alpha_{ij} \left( \frac{V_{ref,i}}{V_{ref,i}^*} - \frac{V_{ref,j}}{V_{ref,j}^*} \right) \\
 \lambda_i \frac{d\delta_i}{dt} &= - \sum_{j \in \mathcal{N}_i} \alpha_{ij} \left( \frac{Q_i}{Q_i^*} - \frac{Q_j}{Q_j^*} \right)
 \end{aligned}$$

where for module  $i$  ( $i = 2, 3, \dots, N$ ) that acts as VCM,  $E_i$ ,  $\delta_i$  are secondary control variables,  $k_i$ ,  $\lambda_i$  are positive gains; for any module  $i$  ( $i = 1, 2, \dots, N$ ),  $V_{ref,i}$  is the amplitude of  $v_{ref,i}$ ,  $Q_i$  is the reactive power output,  $V_{ref,i}^*$  is voltage ratio variable,  $Q_i^*$  is reactive power ratio variable.  $V_{ref,1}^* : V_{ref,2}^* : \dots : V_{ref,n}^*$  is the desired output voltage ratio between modules.  $Q_1^* : Q_2^* : \dots : Q_N^*$  is the desired reactive power ratio between modules. The  $N \times N$  matrix  $A = [\alpha_{ij}]$  is the adjacency matrix of the communication network.  $\mathcal{N}_i$  represents the neighboring set of the module  $i$ .

For the followers, i.e. VCMs, the output voltage is regulated by the secondary controller (5a)-(5c). The open-loop-control voltage reference for VCMs is generated using (5a) with secondary control variables  $E_i$  and  $\delta_i$ . The control gains  $k_i$  and  $\lambda_i$  correspond for the secondary control convergence speed. For the leader, i.e. the CCM, its output voltage is determined by the current controller (1). The secondary controller requires the  $i$ th VCM to obtain  $V_{ref,j}$  and  $Q_j$  from all its neighbors. Thus, the CCM should calculate and share its information to the communication network.

Considering the steady state of the secondary controller, the derivatives should be zero, which is satisfied when

$$\begin{aligned}
 \frac{V_{ref,1}}{V_{ref,1}^*} &= \frac{V_{ref,2}}{V_{ref,2}^*} = \dots = \frac{V_{ref,N}}{V_{ref,N}^*} \\
 \frac{Q_1}{Q_1^*} &= \frac{Q_2}{Q_2^*} = \dots = \frac{Q_N}{Q_N^*}
 \end{aligned}$$

The primary control includes an inner current loop in CCM and open-loop voltage generation in VCMs. The primary control has a much higher control bandwidth, i.e. at least a decade higher than the fundamental frequency. Therefore, for the analysis of secondary control, i.e. power regulation loops, the dynamics of primary control are ignored. Perfect voltage and current reference tracking is assumed, i.e.,

$V_i = V_{ref,i}$  and  $I_g = I^*$ , where  $V_i$  is the amplitude of fundamental component of module  $i$ 's output voltage in steady state and  $V_i$  is the amplitude of fundamental component of converter output current. The output active and reactive power of the  $i$ th module can be presented as:

$$\begin{aligned}
 P_i &= \frac{1}{2} V_i I_g \cos \delta_i = \frac{1}{2} V_{ref,i} I^* \cos \delta_i \\
 Q_i &= \frac{1}{2} V_i I_g \sin \delta_i = \frac{1}{2} V_{ref,i} I^* \sin \delta_i
 \end{aligned}$$

Based on equation (6), (7) and the fact  $\delta_i$  is very small such that  $\sin \delta_i \approx \delta_i$  and  $\cos \delta_i \approx 1$ , it can be further derived that,

$$\frac{P_1}{V_{ref,1}^*} = \frac{P_2}{V_{ref,2}^*} = \dots = \frac{P_N}{V_{ref,N}^*}$$

The proportional power sharing regulation is thus realized by the secondary controller in steady state. As a special case, equal power sharing, as shown in Fig. 4, can be realized if identical  $V_{ref,i}^*$  and  $Q_i^*$  are given for each module.

### B. System Stability Analysis

To verify the stability of the proposed control strategy and derive sufficient conditions for stable operation, the system small signal model and stability analysis are presented. Referring to the secondary controller (5a)-(5c), there are  $2(N - 1)$  state variables,  $E_i$  and  $\delta_i$  ( $i = 2, 3, \dots, N$ ), respectively. Since  $E_1$  and  $\delta_1$  in CCM are not state variables, CCM is separated from system modeling to facilitate the stability analysis. A parameter  $r_i$  is defined to characterize the communication between CCM and other modules. When  $i$ th module communicates directly with CCM,  $r_i = 1$ , otherwise  $r_i = 0$ . The converter under the proposed control scheme can be modeled as:

$$k_i \dot{E}_i = - \sum_{j \in \mathcal{N}_i} \alpha_{ij} \left( \frac{V_{ref,i}}{V_{ref,i}^*} - \frac{V_{ref,j}}{V_{ref,j}^*} \right) - r_i \left( \frac{V_{ref,i}}{V_{ref,i}^*} - \frac{V_{ref,1}}{V_{ref,1}^*} \right)$$

The small-signal model is derived by substituting:

$$k_i \dot{E}_i = - \sum_{j \in \mathcal{N}_i} \alpha_{ij} (E'_i - E'_j) - r_i (E'_i - E'_1) + \Delta_E$$

If taking the approximation that  $\sin \delta_i \approx \delta_i$  and  $V_1 + V_2 + \dots + V_N = V_g$ , i.e.,  $E_1 + E_2 + \dots + E_N = 0$ ,  $E_1$  in CCM can be expressed as:

$$E_1 = - \sum_{i=2}^N E_i$$

If the speed of controller (5c) is designed as much faster than that of controller (5b), it can be assumed that  $E_1 = E_2 = \dots = E_N = 0$  for angle stability analysis. According to (7b),

$$Q_i = \frac{\hat{V}_g I^*}{2N} \delta_i$$

From the system voltage vector diagram, it can be obtained that

$$V_g + j\omega L_f I^* = \sum_{i=1}^N \frac{\hat{V}_g}{N} (\cos \delta_i + j \sin \delta_i)$$

Due to the same imaginary part and small power factor angle,  $\delta_1$  in CCM can be presented as:

$$\delta_1 = \frac{N\omega L_f I^*}{\hat{V}_g} - \sum_{i=2}^N \delta_i$$

The model of converter system with the proposed controller can be summarized as

$$\begin{cases} k_i \dot{E}_i = - \sum_{j \in \mathcal{N}_i} \alpha_{ij} \left( \frac{E_i}{V_{ref,i}^*} - \frac{E_j}{V_{ref,j}^*} \right) - r_i f(E_i) + \Delta_E \\ \lambda_i \dot{\delta}_i = \frac{\hat{V}_g I^*}{2N} \left[ - \sum_{j \in \mathcal{N}_i} \alpha_{ij} \left( \frac{\delta_i}{Q_i^*} - \frac{\delta_j}{Q_j^*} \right) - r_i f(\delta_i) \right] + \Delta_\delta \end{cases}$$

that is irrelevant to system states.

The system model could be written in matrix form:

$$\dot{\mathbf{x}} = \mathbf{W}\mathbf{x} + \mathbf{u}$$

where  $\mathbf{x} = [E \ \delta]^T$  represents system state variables under analysis and the system matrix  $\mathbf{W}$  is

$$\mathbf{W} = \begin{bmatrix} -k_i^{-1} \mathbf{W}_E & \mathbf{0}_{N-1} \\ \mathbf{0}_{N-1} & -\lambda_i^{-1} \frac{\hat{V}_g I^*}{2N} \mathbf{W}_\delta \end{bmatrix}$$

where  $\mathbf{0}_{N-1}$  represents a  $(N - 1)$ -by- $(N - 1)$  zero matrix;

$$\begin{aligned} \mathbf{W}_E &= (\mathbf{L} + 2\mathbf{R}) \begin{bmatrix} \mathbf{1} \\ \mathbf{V}_{ref,i}^* \end{bmatrix} + \frac{1}{V_{ref,1}^*} \mathbf{R}[\mathbf{1}]_{N-1} \\ \mathbf{W}_\delta &= (\mathbf{L} + 2\mathbf{R}) \begin{bmatrix} \mathbf{1} \\ \mathbf{Q}_i^* \end{bmatrix} + \frac{1}{Q_1^*} \mathbf{R}[\mathbf{1}]_{N-1} \end{aligned}$$

where  $\begin{bmatrix} \mathbf{1} \\ \mathbf{V}_{ref,i}^* \end{bmatrix} = \text{diag} \left( \frac{1}{V_{ref,i}^*} \right)$  and  $\begin{bmatrix} \mathbf{1} \\ \mathbf{Q}_i^* \end{bmatrix} = \text{diag} \left( \frac{1}{Q_i^*} \right)$

are diagonal matrices;  $\mathbf{L}$  is the Laplacian matrix of an undirected communication graph with  $(N - 1)$  vertices, which represents the communication network structure among modules;  $\mathbf{R} = \text{diag}(r_i)$  reflects the communication structure between CCM and VCMs;  $[\mathbf{1}]_{N-1}$  represents a  $(N - 1) \times (N - 1)$  all ones matrix;  $\mathbf{V}_{ref,1}^*$  and  $\mathbf{Q}_1^*$  are constants.

The system is exponentially stable if and only if all the eigenvalues of  $\mathbf{W}$  have strictly negative real parts. From the sufficient condition for system stability is that the matrix  $\mathbf{W}_E$  and  $\mathbf{W}_\delta$  are positive definite, i.e. the quadratic form of  $\mathbf{W}_E$  and  $\mathbf{W}_\delta$  is always greater than 0.

Thus, the quadratic form of the matrix  $(\mathbf{L} + 2\mathbf{R})$  can be written as:

$$\mathbf{X}^T (\mathbf{L} + 2\mathbf{R}) \mathbf{X} = \frac{1}{2} \sum_{i,j=1}^{N-1} \alpha_{ij} (x_i - x_j)^2 + \sum_{i=1}^{N-1} r_i x_i^2$$

Similarly,  $\mathbf{W}_\delta$  can be derived to be a positive definite matrix by the same approach. Therefore, the proposed control scheme is stable if a connected communication structure is satisfied.

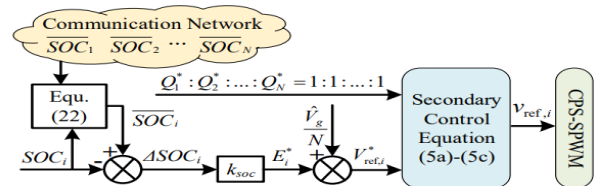


Fig.5: The block diagram of SOC balancing control

### 3.3.3 Battery Soc Balancing Control

For a BESS, the SOC values of different battery modules may diverge from each other due to different operation demands, self-discharging rates, operating temperature, etc. The battery SOC imbalance can result in degraded utilization and overdischarge/overcharge for some batteries. To avoid this issue, the proposed distributed control is utilized to achieve the battery SOC balancing. The control block diagram of SOC balancing is shown in Fig. 3.5.

The average SOC of all battery modules,  $\overline{SOC}_i$ , is estimated in each module using dynamic average consensus algorithm, which is able to track the average of a set of time-varying states in a distributed manner,

$$\dot{\overline{SOC}}_i(t) = \dot{SOC}_i(t) - \sum_{i,j \in N_i} \alpha_{ij} [\overline{SOC}_i(t) - \overline{SOC}_j(t)]$$

In steady state, it can be satisfied that

$$\overline{SOC}_i(t) = \frac{1}{N} \sum_{j=1}^N SOC_j(t)$$

With the estimated average  $\overline{SOC}$ , the difference between estimated average and the actual SOC value of each battery module can be obtained as  $\Delta SOC_i$ . Then,  $\Delta SOC_i$  is used in (24) to obtain the voltage ratio variable,  $V_{ref,i}^*$ .

$$V_{ref,i}^* = k_{soc} \Delta SOC_i + \frac{\hat{V}_g}{N} = k_{soc} (\overline{SOC}_i - SOC_i) + \frac{\hat{V}_g}{N}$$

Then,  $V_{ref,i}^*$  is used in the active power secondary controller (5b) to generate the secondary control variable  $E_i$ . The reactive power ratio is set to be  $Q^* 1 : Q^* 2 : \dots : Q^* N = 1 : 1 : \dots : 1$  to share the reactive power equally among modules. If all components are assumed to be lossless, for each module, the battery power is equal to its output power,

$$V_{bi} I_{bi} = P_i = \frac{P_i^*}{\sum_{i=1}^N P_i^*} \left( \frac{1}{2} V_g I^* \right)$$

The current flowing through the battery module  $i$  is also related to the battery SOC by

$$I_{bi} = C \left( \frac{dSOC_i}{dt} \right)$$

where  $C$  is the nominal capacity of the battery modules.

## V RESULT AND DISCUSSION

Only primary control is enabled to validate the performance of the CPS control. The current reference amplitude  $I^*$  is set to 10 A. In the first case, no CPS control is implemented. The phase difference between different modules becomes timevarying. When the CPS control described in Section V-B is activated, the output voltage of the three modules have a fixed phase shift  $2\pi/3$  as shown in Fig. 10. In both cases, the output current is well controlled, which indicates that the presented primary control has a good current tracking performance. The implemented CPS control can achieve a multilevel voltage output and a lower current ripple.

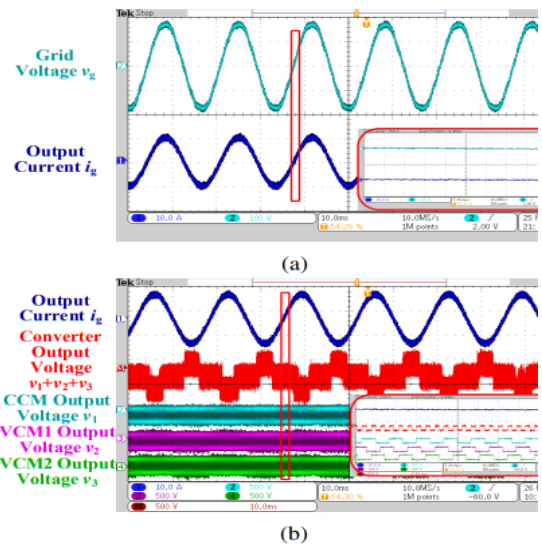


Fig. 6: Waveforms with CPS control when only primary control enabled

We validated the proposed distributed control using both a full and a sparse communication network. In the full communication network, CCM, VCM1 and VCM2 exchange information with each other. In the sparse communication network, CCM only exchanges data with VCM1, and VCM2 only communicates with VCM1. First, the secondary control is activated with primary control and CPS control enabled.

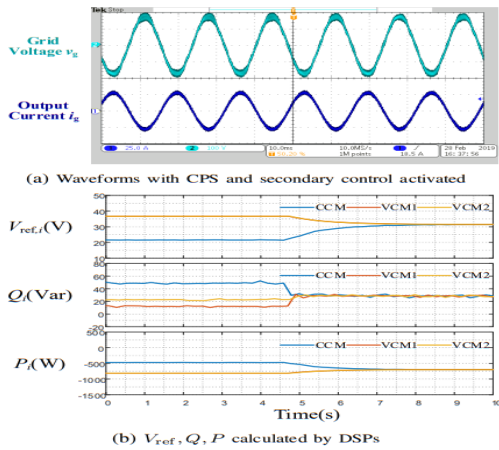


Fig.7: Experiment results when secondary control activated under the full communication network with  $I^* = -28A$

The ratios of  $V^*_{ref}$  and  $Q^*$  are set to be 1: 1: 1 to realize equal power sharing among modules. The experiment results are shown in Fig. 7. Comparing Fig. 7a with Fig. 6, it can be found that the current tracking performance is still good after activating the secondary control. Data transmitted in the communication network are recorded and plotted in Fig. 7b. Besides, the dynamic performance of the proposed control scheme is tested by stepping the current reference amplitude  $I^*$  from -10 A to 20 A. The transient responses of the output current and output voltage are shown in Fig. 8a and the secondary control responses are shown in Fig. 8b. The output current can follow the reference step change in about 800  $\mu s$ . Equal active and reactive power sharing among modules is achieved shortly after the transients.

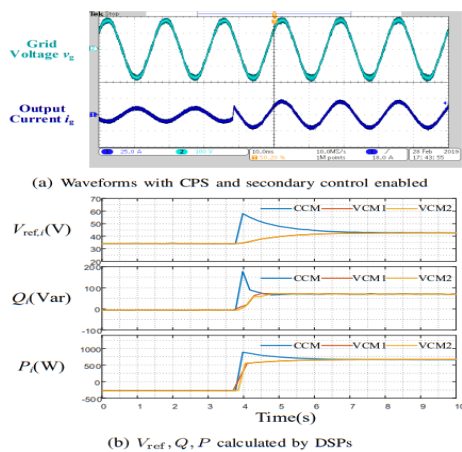


Fig. 7: Experimental results when  $I^*$  steps from -10A to 20A under the full communication network

## VI CONCLUSION AND FUTURE WORK

In this paper, we propose a hierarchical distributed control architecture for CHB converter, which consisting of three levels - primary control, secondary control and battery SOC balancing control. The primary control is in charge of ensuring output current tracking and maintaining the stability of the grid-connected operation of BESS. The secondary control based on consensus algorithm achieves power sharing regulation among modules and is proved to be stable. Battery SOC balancing is further realized based on the secondary control and dynamic average consensus algorithm in a distributed manner. Moreover, the proposed control strategies, along with the CPS control, are implemented in a CHB converter testbed and validated through experiment.

## VII REFERENCES

- [1] G. Wang, G. Konstantinou, C. D. Townsend, J. Pou, S. Vazquez, G. D. Demetriades, and V. G. Agelidis, "A review of power electronics for grid connection of utility-scale battery energy storage systems," *IEEE Transactions on Sustainable Energy*, vol. 7, no. 4, pp. 1778–1790, 2016.
- [2] Z. Ye, L. Jiang, Z. Zhang, D. Yu, Z. Wang, X. Deng, and T. Fernando, "A novel dc-power control method for cascaded h-bridge multilevel inverter," *IEEE Transactions on Industrial Electronics*, vol. 64, no. 9, pp. 6874–6884, 2017.
- [3] E. Villanueva, P. Correa, J. Rodriguez, and M. Pacas, "Control of a single-phase cascaded h-bridge multilevel inverter for grid-connected photovoltaic systems," *IEEE Transactions on Industrial Electronics*, vol. 56, no. 11, pp. 4399–4406, 2009.
- [4] H. Zhao, T. Jin, S. Wang, and L. Sun, "A real-time selective harmonic elimination based on a transient-free inner closed-loop control for cascaded multilevel inverters," *IEEE Transactions on Power Electronics*, vol. 31, no. 2, pp. 1000–1014, 2016.
- [5] H. Jafarian, R. Cox, J. H. Enslin, S. Bhowmik, and B. Parkhideh, "Decentralized active and reactive power control for an ac-stacked pv inverter with single member phase compensation," *IEEE Transactions on Industry Applications*, vol. 54, no. 1, pp. 345–355, 2018.
- [6] H. Hu, X. She, and A. Q. Huang, "Decentralized architecture and control of photovoltaic generation system based on cascaded ac module integrated converter," in *2014 IEEE Energy Conversion Congress and Exposition (ECCE)*, 2014, pp. 2280–2287.

- [7] P. Wu, Y. Su, J. . Shie, and P. Cheng, "A distributed control technique for the multilevel cascaded converter," *IEEE Transactions on Industry Applications*, vol. 55, no. 2, pp. 1649–1657, 2019.
- [8] N. Kim and B. Parkhideh, "Control and operating range analysis of an ac-stacked pv inverter architecture integrated with a battery," *IEEE Transactions on Power Electronics*, vol. 33, no. 12, pp. 10 032–10 037, 2018
- [9] P. Poblete, J. Pereda, F. Nuez, and R. P. Aguilera, "Distributed current control of cascaded multilevel inverters," in *2019 IEEE International Conference on Industrial Technology (ICIT)*, 2019, pp. 1509–1514.
- [10] B. P. McGrath, D. G. Holmes, and W. Y. Kong, "A decentralized controller architecture for a cascaded h-bridge multilevel converter," *IEEE Transactions on Industrial Electronics*, vol. 61, no. 3, pp. 1169– 1178, 2014.
- [11] P. K. Achanta, D. Maksimovic, and M. Ilic, "Decentralized control of series stacked bidirectional dc-ac modules," in *2018 IEEE Applied Power Electronics Conference and Exposition (APEC)*, 2018, pp. 1008–1013.
- [12] B. Xu, H. Tu, Y. Du, H. Yu, H. Liang, and S. Lukic, "A distributed control architecture for cascaded h-bridge converter," in *2019 IEEE Applied Power Electronics Conference and Exposition (APEC)*, 2019, pp. 3032–3038.
- [13] M. A. Awal, H. Yu, I. Husain, W. Yu, and S. Lukic, "Decentralized synchronization of ac-stacked voltage source converters," in *2018 IEEE Energy Conversion Congress and Exposition (ECCE)*, 2018, pp. 4895– 4901.
- [14] L. Zhang, K. Sun, Z. Huang, and Y. W. Li, "A grid-tied photovoltaic generation system based on series-connected module integrated inverters with adjustable power factor," in *2015 IEEE Energy Conversion Congress and Exposition (ECCE)*, 2015, pp. 6864–6870.
- [15] W. Huang and J. A. Abu Qahouq, "Energy sharing control scheme for state-of-charge balancing of distributed battery energy storage system," *IEEE Transactions on Industrial Electronics*, vol. 62, no. 5, pp. 2764– 2776, 2015.
- [16] L. Maharjan, S. Inoue, H. Akagi, and J. Asakura, "State-of-charge (soc)- balancing control of a battery energy storage system based on a cascade pwm converter," *IEEE Transactions on Power Electronics*, vol. 24, no. 6, pp. 1628–1636, 2009.
- [17] M. Vasiladiotis and A. Rufer, "A modular multiport power electronic transformer with integrated split battery energy storage for versatile ultrafast ev charging stations," *IEEE Transactions on Industrial Electronics*, vol. 62, no. 5, pp. 3213–3222, 2015.
- [18] X Hou, Y Sun, H Han, et al. (2019) A fully decentralized control of grid-connected cascaded inverters. *IEEE Transactions on Sustainable Energy*, 10(1): 315-317
- [19] W Huang, J A Qahouq (2015) Energy sharing control scheme for state-of-charge balancing of distributed battery energy storage system. *IEEE Transactions on Industrial Electronics*, 62(5): 2764- 2776
- [20] L Maharjan, S Inoue, H Akagi, et al. (2009) State-of-charge (SOC)-balancing control of a battery energy storage system based on a cascade PWM converter. *IEEE Trans. Power Electron*, 24(6): 1628-1636
- [21] J He, X Liu, C Mu, et al. (2020) Hierarchical control of seriesconnected string converter-based islanded electrical power system. *IEEE Transactions on Power Electronics*, 35(1): 359-372
- [22] B Xu, H Tu, Y Du, et al. (2021) A distributed control architecture for cascaded h-bridge converter with integrated battery energy storage. *IEEE Transactions on Industry Applications*, 57(1): 845- 856